

# Dynamical witnesses and universal behavior across chaos and non-ergodicity in the tilted Bose–Hubbard model

Carlos Diaz-Mejia,<sup>1</sup> Sergio Lerma-Hernández,<sup>2</sup> and Jorge G. Hirsch<sup>1</sup>

<sup>1</sup>*Instituto de Ciencias Nucleares, Universidad Nacional Autónoma de México,  
Apdo. Postal 70-543, C.P. 04510 CDMX, Mexico*

<sup>2</sup>*Facultad de Física, Universidad Veracruzana, Campus Arco Sur,  
Paseo 112, C.P. 91097 Xalapa, Veracruz, Mexico*

(Dated: February 3, 2026)

Quantum chaos in isolated quantum systems is intimately linked to thermalization and the rapid relaxation of observables. Although the spectral properties of the chaotic phase in the tilted Bose–Hubbard model have been well characterized, the corresponding dynamical signatures across the transition to regularity remain less explored. In this work, we investigate this transition by analyzing the time evolution of the survival probability, the single-site entanglement entropy, and the half-chain imbalance. Our results reveal a clear hierarchy in the sensitivity of these observables: the relaxation value of the entanglement entropy varies smoothly as a function of the Hamiltonian parameters across the chaos-regular transition, while the imbalance exhibits a more pronounced distinction. Most notably, the survival probability emerges as the most robust indicator of the transition between chaos and regularity. When appropriately scaled, all three observables converge onto a common behavior as a function of the Hamiltonian parameters for different numbers of sites and bosons, enabling a universal characterization of the transition between chaotic and regular dynamics.

## I. INTRODUCTION

The question of how closed quantum systems thermalize is fundamentally tied to the concepts of quantum chaos and ergodicity[1–4]. According to the Eigenstate Thermalization Hypothesis (ETH)[2], the eigenstates of chaotic, non-integrable Hamiltonians enable subsystems to thermalize, while integrable systems with extensive conserved quantities evade thermalization. The tilted Bose–Hubbard model (TBH) has emerged as a paradigmatic system for studying this interplay, as its parameters allow one to tune between integrable and chaotic regimes [5–7]. Its integrable limits are well-known: localized Fock states for zero hopping ( $J = 0$ ), Wannier-Stark states for zero interaction ( $U = 0$ ) and momentum- $k$  states for hopping dominating interaction and tilt terms ( $J \gg U, D$ )[8]. The non-integrable region hosts a rich and tunable chaotic phase. Recent work has meticulously mapped the static properties of this chaotic phase[5] providing a comprehensive characterization of the chaotic regime through the spectral statistics and the multi-fractal properties of eigenvectors. However, other fundamental implications of quantum chaos are dynamical. While spectral analysis identifies the existence of a chaotic regime, it does not directly reveal how the transition into and out of this regime is experienced by a quantum state evolving in time. A crucial question is: how does the breakdown of ergodicity, as one moves from the chaotic phase towards the integrable limits, manifests in the real-time dynamics of experimentally accessible observables? In this work, we fill this gap by investigating the dynamical signatures of the transition from quantum chaos to regularity in the TBH.

We numerically simulate the non-equilibrium quantum quench dynamics from averages over Fock ini-

tial states, monitoring key observables that are directly probed in cold-atom experiments[9–13]: the survival probability[14–17], the entanglement entropy, and the imbalance.

Our results show that these quantities, each with its own sensitivity, act as dynamical indicators of the underlying regular-chaos transition. We show that when interaction and tilt are similar ( $U \sim D \sim J$ ), the dynamics exhibit rapid decay of survival probability and fast relaxation of entanglement entropy and imbalance,—all consistent with thermalization in the chaotic ergodic phase. In contrast, when the tilt dominates ( $D \gg U$ ), Wannier-Stark Localization (WSL)[18–20] takes place, the dynamics are starkly different, showing deep oscillations in the survival probability and entanglement entropy and slow loss of memory of the initial state—hallmarks of a non-ergodic, regular regime. By tracking the temporal behavior of these observables, we dynamically trace the boundary between chaos and regularity, providing a complementary and experimentally actionable perspective on the phase diagram established by static measures.

This paper is organized as follows. Sec. II introduces the tilted Bose–Hubbard Hamiltonian. Section III defines the observables used in our analysis and examines the static properties of the Hamiltonian eigenstates across the transition between chaos and regularity. In Sec. IV, we present the distinct dynamical responses of these observables as the system moves from the chaotic regime toward the interaction-dominated and tilt-dominated limits, and we characterize the dynamical signatures of this transition using averages over Fock initial states. Finally, we present our conclusions in Sec. V.

## II. THE MODEL

We analyze the one-dimensional tilted Bose-Hubbard model with  $N$  bosons on  $M = N$  sites and open boundary conditions[5, 7, 21, 22],

$$H = -J \sum_{i=1}^{M-1} (\mathbf{b}_i^\dagger \mathbf{b}_{i+1} + \text{h.c.}) + \sum_{i=1}^M \left[ \frac{U}{2} \mathbf{n}_i (\mathbf{n}_i - \mathbf{1}) + D i \mathbf{n}_i \right] \quad (1)$$

where  $\mathbf{b}_i^\dagger$  ( $\mathbf{b}_i$ ) are the bosonic creation (annihilation) operators at site  $i$ , and  $\mathbf{n}_i = \mathbf{b}_i^\dagger \mathbf{b}_i$  is the number operator. The Hilbert space dimension is  $\mathcal{D}(N, M) = (M + N - 1)!/(N!(M - 1)!)$ . The model is governed by three parameters: the tunneling amplitude  $J$ , the on-site interaction  $U$ , and the tilt  $D$ . Because the tilt breaks the parity symmetry, particle number is the only remaining conserved quantity.

Throughout this work we set  $J = 1$  as the unit of energy and explore the model by varying  $U$  and  $D$ . We characterize the transition from integrability to quantum chaos using both local and non-local dynamical observables. A recent detailed study has analyzed the interplay of these parameters using level statistics and multifractal analysis[5]. As noted above, the system possesses integrable limits: when  $U \rightarrow 0$ , the system admits analytical solutions known as Wannier-Stark states and dynamically exhibits Bloch oscillations [23, 24]. When  $D \rightarrow 0$ , one recovers the standard Bose-Hubbard system[17, 25], which itself has two integrable limits. For  $U \gg J$ , the system maps onto free fermion (the Hard-Core Boson limit, HCB). For  $J \gg U$ , the system becomes that of free, non-interacting bosons in a tight-binding chain, diagonal in momentum space.

We investigate the behavior of the model as the tilt is increased (at fixed interaction), tracing the progression from the chaotic Bose-Hubbard regime through the chaotic tilted Bose-Hubbard regime and finally into the integrable Wannier-Stark Localization limit—that is, the cBH-cTBH-WSL transition (vertical line in Fig.1). Complementarily, we examine the path where the interaction strength is increased (at fixed tilt), driving the system from the integrable Wannier-Stark-localization regime, through the chaotic Tilted Bose-Hubbard regime and ultimately into the integrable Hard-Core Bosons limit, corresponding to the WSL-cTBH-HCB transition (horizontal line in Fig.1).

## III. STATIC SIGNATURES OF THE TRANSITION CHAOS TO REGULARITY.

### A. Quantum chaos

We adopt the standard quantum-chaos criterion based on the similarity between eigenenergy correlations and those of an appropriate random-matrix ensemble, which for the present model corresponds to the Gaussian

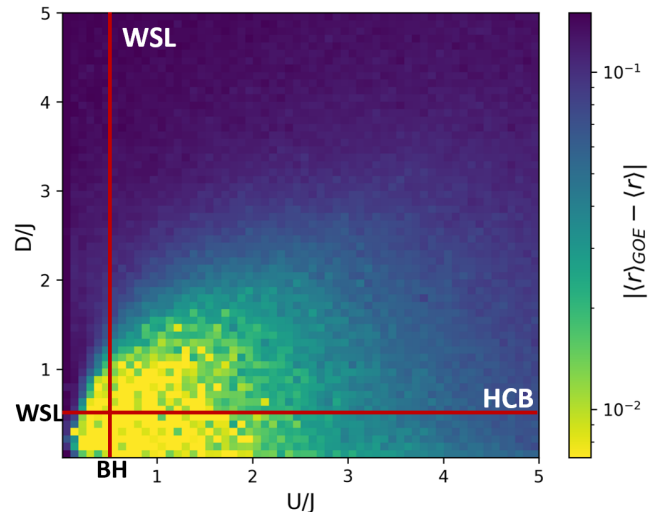


Figure 1. Absolute value of the difference between the mean level-spacing ratio  $\langle r \rangle$  of the eigenspectrum of the tilted Bose-Hubbard model and the chaotic GOE prediction, shown as a function of the interaction  $U/J$  and the tilt for a system with  $N = M = 8$ . The red lines indicate the parameter paths explored in the numerical simulations. The acronyms indicate the following limits: WSL (the integrable Wannier-Stark Localization ), HCB (the integrable HardCore Bosons), and BH (the chaotic Bose-Hubbard model at  $D = 0$ ).

Orthogonal Ensemble (GOE). Quantum chaotic systems exhibit unfolded level spacings  $\tilde{s}_n = (E_{n+1} - E_n)\rho(\bar{E}_n)$ , where  $\rho(E)$  is the density of states and  $\bar{E}_n = (E_{n+1} + E_n)/2$ , that follows the Wigner-Dyson distribution, whose main characteristic is level repulsion ( $\lim_{\tilde{s} \rightarrow 0} P(\tilde{s}) = 0$ ) [3, 14]. To avoid the unfolding procedure, one can instead use the mean ratio of consecutive level spacings [26][27]

$$\langle r \rangle = \left\langle \frac{\min(s_n, s_{n-1})}{\max(s_n, s_{n-1})} \right\rangle, \quad (2)$$

where  $s_n = E_{n+1} - E_n$ . This ratio is independent of the density of states, making unfolding unnecessary. For quantum-chaotic systems, the mean level spacing ratio is  $\langle r \rangle_W \approx 0.535$ , while regular spectra yield the lower value  $\langle r \rangle_P \approx 0.386$ .

Our analysis of the mean level spacing ratio,  $\langle r \rangle$ , reveals a rich structure in the chaos-regularity phase diagram as a function of interaction strength  $U$  and tilt  $D$  (Fig. 1). For very small tilt  $D \approx 0$ , the symmetry sectors of the non-tilted Bose-Hubbard model are broken, and the mean spacing ratio  $\langle r \rangle$  exhibits GOE behavior for  $U/J \in [0.1, 2]$ . This agrees with known results for the non-tilted Bose-Hubbard model, where each parity sector displays GOE correlations over the same interval[25]. A similar breaking of parity symmetry occurs in the interacting Aubry-André model when a very weak onsite disorder is introduced[28].

The onset of chaotic behavior shows a pronounced asymmetry in the systems' response to the two parame-

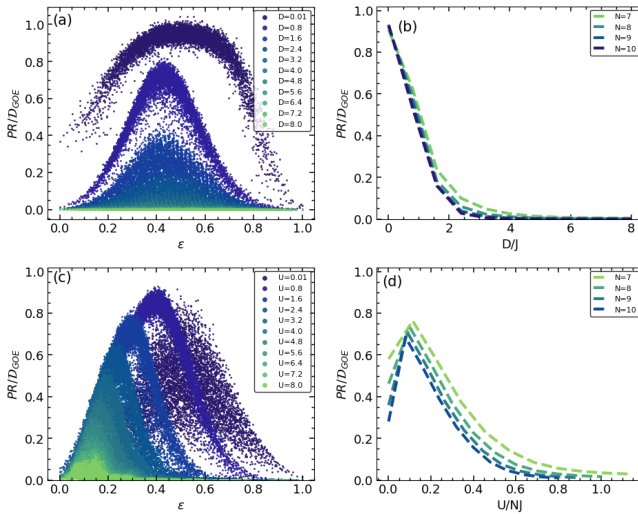


Figure 2. Left:  $PR/D_{GOE}$  of the eigenstates in the Fock basis for  $N = 8$ . Right: scaling analysis averaging over 80% of the eigenstates in the center of the spectrum. In the upper panel, interaction is fixed at  $U = 0.5J$  and  $D$  varied; in the lower panel, tilt is fixed at  $D = 0.5J$  and  $U$  varied.

ters: chaos is rapidly suppressed as  $D$  increases at fixed  $U$ , whereas it remains much more robust when  $U$  is increased at fixed  $D$ . As we demonstrate below, this asymmetry is also reflected in the dynamical observables.

## B. Participation ratio

The participation ratio (PR) of a normalized state  $|\Psi\rangle = \sum_k c_k |k\rangle$  expanded in an orthonormal basis  $\{|k\rangle\}$ , is defined as

$$PR = \frac{1}{\sum_k |c_k|^4}. \quad (3)$$

The PR quantifies how delocalized the state  $|\Psi\rangle$  is within the chosen basis. When a state  $|\Psi\rangle$  is evenly distributed in the basis, the PR is as large as the dimension ( $\mathcal{D} = \mathcal{D}(N, M)$ ) of the Hilbert space, whereas a state localized in a single basis element has  $PR = 1$ . In chaotic regimes where eigenstates resemble those of the Gaussian orthogonal ensemble, one expects  $PR \approx \mathcal{D}_{GOE} = \mathcal{D}/3$  [29].

To allow a consistent comparison across systems with different tilts and interaction strengths, we present our results in terms of the normalized energy,

$$\epsilon = \frac{E - E_{min}}{E_{max} - E_{min}}. \quad (4)$$

Fig. 2 shows how the participation ratios of the eigenstates in the Fock basis change as the interaction or tilt varies. In panel (a), for very small tilt ( $D = 0.01$ ), chaos arises throughout the spectrum, and the participation ratio behaves as a smooth function of energy with low

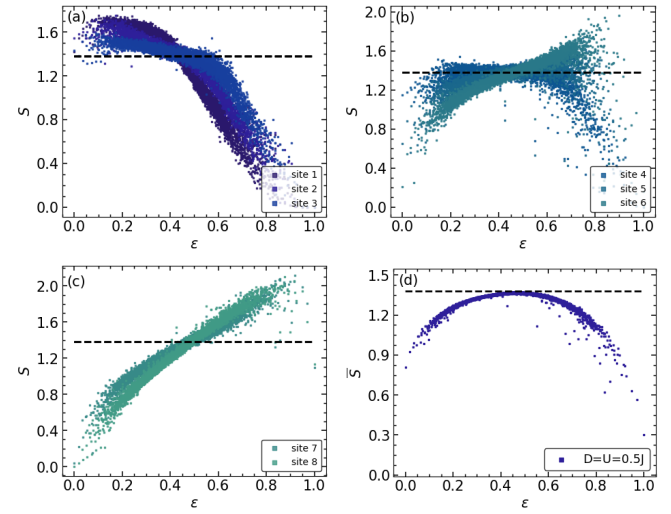


Figure 3. Single-site entanglement entropy of eigenstates for  $N = 8$ . Panels (a)–(c) show  $S^{(i)}$  grouped by sites (from edge to middle), revealing how spatial position and energy density shape the entanglement landscape; panel (d) displays the site average  $\bar{S}$ . The black dashed line is the Page value. Parameters are chosen in the chaotic window, where most mid-spectrum eigenstates are near-thermal yet site-dependent deviations persist.

dispersion of values. Only the eigenstates at the edges of the spectrum —those with very high and very low energy— display low small PR values, indicating stronger localization in the Fock basis. As the tilt increases, the PR decreases uniformly across the spectrum, consistent with a system entering the Wannier-Stark-Localization regime. This trend is also reflected in the scaling analysis shown in panel (b). It is worth noting that the larger the system, the more sensitive it becomes to the Wannier-Stark-Localization (WSL) transition as the tilt increases.

Panel (c) of Figure 2, reveals a different behavior when the interaction strength is varied. Two integrable limits are expected: 1) when the interaction approaches zero (Wannier-Stark eigenstates), the PR exhibits a wide dispersion of values across all the energy range, and 2) when interaction dominates, we have the HCB integrable regime. Within the chaotic regime ( $U \in [0.8, 2]J$ ), the PR behaves smoothly as a function of energy. The PR of eigenstates with higher energy rapidly decay, while the eigenstates in the middle of the spectrum present values of PR organized in a narrow band extending through the low-energy region of the spectrum. The scaling analysis in panel (d) shows that adding more bosons does not qualitatively change this trend, but the transition toward the HCB integrable regime becomes more pronounced as the number of bosons increases.

A noteworthy observation from the scaling analysis in the right panels of Fig 2 is the striking similarity of the curves across all examined system sizes. This collapse is achieved by appropriately scaling the variables: the participation ratio is normalized by the GOE reference value

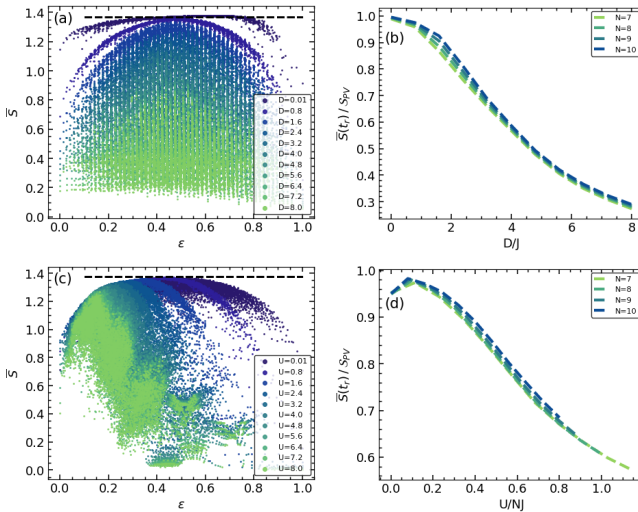


Figure 4. Left:  $\bar{S}$  of the eigenstates in the Fock basis for  $N = 8$ , the black dashed line is the Page value  $S_P$ . Right:  $\bar{S}/S_P$  scaling analysis averaging over 80% of the eigenstates in the center of the spectrum. In the upper panel, interaction is fixed at  $U = 0.5J$ ; in the lower panel, tilt is fixed at  $D = 0.5J$ . Single-site entanglement entropy of eigenstates for  $N = 8$ .

$D_{GOE} = \mathcal{D}/3$ , and the interaction strength is rescaled by the number of bosons  $N$ , consistent with the two-body nature of the interaction term. It is also interesting that the participation ratio of the eigenstates does not reach the GOE expectation, i.e.,  $PR/\mathcal{D}_{GOE} < 1$ .

### C. Entanglement Entropy

The entanglement entropy of eigenstates is a widely used observable [10, 18] for characterizing thermalization [12], quantum chaos[30], non-thermal behavior such as many-body scars[31], and many-body localization transitions[13]. In this section, we employ it to analyze the crossover between integrability and chaos, first for the eigenstates and later in Sec.IV for the dynamics of initial Fock states.

We consider the entanglement entropy between a single site and the rest of the chain. Since we are considering a tilted non-periodic chain, each site is inequivalent and no site is preferred. To obtain a consensus indicator of chaotic versus regular behavior, we average the entanglement entropy over all single-site subsystems. It is important to note, however, that the entanglement entropy of different individual sites conveys complementary information.

For any site  $i$ , the single-site entanglement entropy is defined as

$$S^{(i)} = -\text{Tr}[\rho_i \ln \rho_i], \quad \rho_i = \text{Tr}_{\bar{i}} \rho, \quad (5)$$

where the second trace is taken over the complement of site  $i$  (the remaining  $M-1$  sites, denoted as  $\bar{i}$ ) and  $\rho$  is

the pure-state density matrix of the entire system. The average over all sites is

$$\bar{S} = \frac{1}{M} \sum_{i=1}^M S^{(i)}. \quad (6)$$

When this average is taken, the expected typical entanglement entropy for chaotic states in systems with conserved particles was calculated in Ref.[32] as

$$S_{PV} = Vf[(n+1)\ln(n+1) - n\ln n] + 1/2(f + \ln(1-f)), \quad (7)$$

where  $f = 1/M$  is the subsystem fraction,  $n = N/V$  is the particle density and  $V = M$  is the volume of the system. We refer to this quantity as the Page value.  $S_{PV}$  serves as an upper bound for the averaged entanglement entropy and provides an important reference value for the following analysis.

In Fig. 3 we examine how the entanglement entropy of single sites varies from the bottom site  $S^{(1)}$  to the highest site  $S^{(M)}$ , for  $M = N = 8$  in a chaotic regime with  $U/J = D/J = 0.5$ . Sites are grouped into three sets: in panel(a) the first three sites display very similar entanglement, reflecting boundary effects. High-energy eigenstates are less likely to exhibit large entanglement. In panel (b) the entanglement entropy of sites 4,5 and 6 exhibits a reduced dispersion of values for states near the center of the spectrum. Nevertheless, some of these eigenstates appear as athermal outliers of ETH expectations. In panel (c) the entanglement entropy of sites 7 and 8 again reveals boundary effects, with high-energy states exhibiting large entanglement. Finally, in panel (d) the average over all sites shows very low dispersion, consistent with ETH. At low and high energies, the averaged entropy is reduced compared to the central region, where it approaches the Page value  $S_{PV}$ . Yet, athermal outliers remain visible in the chaotic center of the spectrum.

The averaged one-site entanglement entropy provides a useful diagnostic of the transition between regular and chaotic regimes. The upper panels of Figure 4 illustrate how this transition evolves as the tilt strength increases from weak to strong. In panel (a), we present the averaged entanglement entropy of all eigenstates for a fixed interaction strength  $U = 0.5J$  and varying tilt  $D$ . At  $D = 0.01$ , the system is close to the chaotic Bose Hubbard limit; correspondingly, the entanglement entropy is high for most eigenstates and exhibits low dispersion. As the tilt increases ( $D = 0.8$  and  $D = 1.6$ ), eigenstates away from the center of the spectrum begin to show entropy values below the Page value  $S_{PV}$ . For even larger tilt strengths, the entanglement entropy decreases uniformly, and degeneracies in the energy spectrum become evident. Nevertheless, unlike the participation ratio, entanglement entropy does not exhibit an abrupt change at higher tilt strengths.

The previous behavior is highlighted by comparing panel (b) of Fig.4 with the corresponding panel (b) of

Fig. 2. In Fig.4(b), the mean entanglement entropy of eigenstates in the middle of the spectrum is plotted as a function of the ratio  $D/J$  for system sizes  $N = M = 7, 8, 9$  and  $10$ . Remarkably, when the mean entanglement entropy is rescaled by the corresponding Page value  $S_{PV}$ , the resulting curves collapse onto one another, forming a nearly universal curve that is largely independent of system size.

On the other hand, panel (c) of Fig 4 illustrates the effect of varying the interaction strength at a fixed tilt. In this case, higher- energy eigenstates are markedly more sensitive to changes in the interaction, as evidenced by a rapid decrease in their entanglement entropy. For weak interactions ( $U = 0.01, 0.8$  and  $1.6$ ), the entropy values form an arch-like structure; broad and highly dispersed at  $U = 0.01$ , and narrowing at  $U = 0.8$ . This is consistent with the system residing in the regular WSL regime at very low interaction strengths. As the interaction strength increases further and the system crosses into the regular HCB regime ( $U \geq 2.4$ ), the arch-shaped structure disappears and entropy values become significantly more dispersed. However, unlike the PR shown in panel (b) of Fig.2, the entanglement entropy does not drop to values substantially below the corresponding reference value (here  $S_{PV}$ , and  $\mathcal{D}_{GOE}$  in the case of the PR).

In panel (d) of Fig.4, we present the mean entanglement entropy of eigenstates in the center of the spectrum as a function of the rescaled interaction parameter [ $U/(NJ)$ ] for different system sizes. The mean entropy is normalized by the corresponding  $S_{PV}$ , yielding curves that collapse across all all four system sizes considered. As expected, the maximum of this nearly universal curve does not occur at  $U = 0$ , but rather around  $U/(NJ) \approx 0.15$ , in agreement with the chaotic region identified in Fig.1.

#### D. Imbalance

Another well-known observable is the imbalance [18, 33, 34]. As a complement to the entanglement entropy, the imbalance tracks how the boson population distributes across the chain. It is also far more accessible experimentally and effectively distinguishes between chaotic and localized phases. In spin and fermionic systems, the odd–even imbalance is commonly used [34–36]. Here, instead, we employ the half-chain imbalance, defined as

$$\mathcal{I} = \frac{\langle n_l \rangle - \langle n_r \rangle}{N}, \quad (8)$$

where  $n_l = \sum_{i=1}^{\lceil M/2 \rceil} n_i$  and  $n_r = \sum_{i=\lceil M/2 \rceil+1}^M n_i$  are the total particle numbers in the left and right halves of the chain, respectively, and  $\lceil x \rceil$  denotes the nearest integer that is larger than or equal to  $x$ . When the number of sites  $M$  is even, both halves have the same length, while

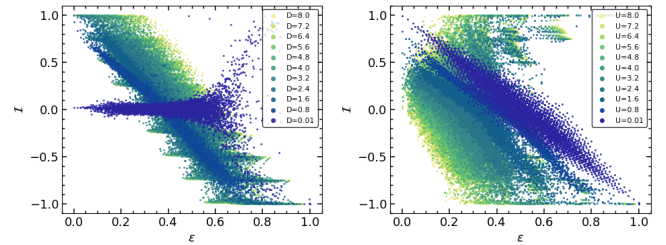


Figure 5. Half-chain imbalance for eigenstates for different tilt strengths at fixed interaction  $U = 0.5J$  (left) and for varying interaction strength at fixed tilt  $D = 0.5J$  (right). As  $D/J$  increases, eigenstates cluster near specific imbalance values, forming a ladder-like structure characteristic of Wannier-Stark Localization tendencies.

for odd  $M$  the right half contains one site fewer than the left.

Figure 5 shows the imbalance as a function of the rescaled energy of the Hamiltonian eigenstates. In panel (a), for  $D = 0.01J$ , the imbalance is narrowly concentrated around zero with small dispersion, except for the highest-energy states. As the tilt increases slightly, the imbalance values spread diagonally across the full interval  $[-1, 1]$ : high-energy states occupying the right half of the chain, while low energy eigenstates occupying the left half. For small tilt, the imbalance remains a smooth function of energy. With further increase in tilt, the diagonal pattern persists but becomes more dispersed, signaling a transition to a non-chaotic regime. At very large tilt, the imbalance organizes into discrete values, forming a ladder-like structure characteristic of Wannier-Stark localization.

Panel (b) displays the imbalance for different interaction strengths at fixed tilt  $D = 0.5J$ . Because the tilt is already large, the imbalance exhibits a diagonal pattern for small interactions. In this parameter region — where the spectral statistics indicate chaotic behavior — the imbalance shows low dispersion and varies smoothly with energy. As the interaction increases, the spectrum compresses toward low energies, and the imbalance values spread vertically, breaking the diagonal structure. Similar to the tilt-dominated regime, some states cluster around specific imbalance values; however, most eigenstates display values with no clear pattern.

#### IV. DYNAMICAL SIGNATURES OF TRANSITION CHAOS TO REGULARITY

Dynamical properties are equally revealing of the regular-to-chaotic crossover. We illustrate this by examining the behavior of three observables as functions of either the interaction strength  $U$  or the tilt  $D$ , while keeping the other fixed and varying it until one of them dominates. The observables we consider are 1) the survival probability, a global measure that directly reveals long-range spectral correlations through the so-called

correlation hole; 2) the on-site entanglement entropy, which grows ballistically and relaxes rapidly in chaotic regimes [30, 37]; and 3) the half-chain imbalance, which also increases or decays to zero very quickly when chaos is prevalent. As the system approaches regularity, these behaviors change significantly: the survival probability lacks the distinctive correlation hole and shows strong initial fluctuations; entanglement growth becomes logarithmic [38]; and the imbalance remains close to its initial value, consistent with WSL behavior.

We analyze the dynamics of these observable using sets of initial Fock product states with on-site occupations restricted to  $n_i \leq 3$  for all  $i = 1, \dots, M$ . Such states are experimentally realistic and have been realized in recent setups (e.g., half filling or two bosons per site) [13, 31, 35]. For the survival probability, and for each of the four system sizes considered, we randomly select 200 Fock states from those whose mean energies lie within the energy interval  $[E_c - 0.4\Delta E_s, E_c + 0.4\Delta E_s]$ , where  $E_c$  and  $\Delta E_s$  are the mean energy and standard deviation, respectively, of the energy spectrum corresponding to the parameters  $U = 0.5J$  and  $D = 0.8J$  — a point well inside the chaotic regime according to the map in Fig.1. This same set of initial Fock states is used throughout our analysis of the survival probability when the Hamiltonian parameters are varied.

For the entanglement entropy, we follow an analogous selection procedure. The only difference is that, due to numerical limitations, we use fewer initial states: specifically, 50 random Fock states for system sizes  $N = M = 7, 8$  and 9, and 20 states for the largest system  $N = M = 10$ .

For the imbalance, we choose initial Fock states that not only satisfy  $n_i \leq 3$  but also have an initial imbalance  $\mathcal{I} = -1$ . These correspond to states with all bosons on the right half of the chain and none on the left. For system sizes  $N = M = 7, 8$  and 9, we use all Fock states satisfying these conditions, which amount to 6, 31 and 20 states, respectively. For the largest system size,  $N = M = 10$ , the number of qualifying states increases to 101; however, due to numerical constraints, we randomly select only 20 states of them.

In the Appendix, we present for the case  $N = M = 8$  the complete set of 50 states used for the entanglement entropy analysis and the set used for the imbalance dynamics.

### A. Survival Probability

The survival probability  $S_P(t)$  (or fidelity) is the probability of finding the system in its initial state  $|\Psi(0)\rangle$  after unitary evolution to  $|\Psi(t)\rangle$ ,

$$S_P(t) = |\langle\Psi(0)|\Psi(t)\rangle|^2 = \left| \sum_m |c_m|^2 e^{-iE_m t} \right|^2, \quad (9)$$

where  $c_m$  are the components of the initial state in the Hamiltonian eigenbasis,  $|\Psi(0)\rangle = \sum_m c_m |E_m\rangle$ . The survival probability is closely related to the spectral form factor (SFF) [39]. It is convenient to decompose  $S_P(t)$  into diagonal and off-diagonal contributions,

$$S_P(t) = \sum_m |c_m|^4 + \sum_{k \neq m} |c_m|^2 |c_k|^2 e^{-i(E_m - E_k)t}. \quad (10)$$

At long times, and in the absence of degeneracies, the temporal average of  $S_P(t)$  approaches the inverse participation ratio of the state in the energy eigenbasis,  $\overline{S_P} = \text{IPR} = \sum_m |c_m|^4$ . In the chaotic region,  $S_P(t)$  develops a pronounced dip before reaching the IPR plateau. This correlation hole is a hallmark of long-range spectral correlations. As a specific instance of the SFF, the survival probability exhibits the standard dip–ramp–plateau structure, which can be described analytically [40],

$$\langle S_P(t) \rangle = \frac{1 - \text{IPR}}{\eta - 1} \left[ \eta S_P^{bc}(t) - b_2 \left( \frac{t}{2\pi\bar{\nu}} \right) \right] + \text{IPR}, \quad (11)$$

where  $S_P^{bc}(t)$  is the squared modulus of the Fourier transform of the smoothed local density of states,  $S_P^{bc}(t) = \left| \int dE \rho(E) e^{-iEt} \right|^2$ ,  $\bar{\nu}$  is the mean density of states in the energy region where the dominant components  $c_m$  lie,  $\eta = (\int dE \rho^2(E)/\nu(E))^{-1}$  quantifies the effective number of levels involved and  $b_2(\tau)$  is the GOE two-level form factor. The survival probability has emerged as a practical quantum indicator of chaos, since for random initial states its late dynamics can be directly related to the GOE two-level form factor [15–17, 41]. Figure 6 shows an example of a typical survival-probability curve in a chaotic regime along with the corresponding analytical prediction. The correlation hole appears at middle times ( $t \in [20, 10^3]$ ). The expected value of the survival probability at the minimum of the correlation hole can be estimated using GOE matrices [42], yielding  $S_{P\min} \approx 2/\mathcal{D}$ . Combined with the GOE estimate for the IPR,  $\text{IPR} = 1/\text{PR} = 3/\mathcal{D}$ , we obtain an estimate of the depth of the correlation hole  $|S_{P\min} - \text{IPR}| \approx 1/\mathcal{D}$ . Since this value is very small, it is more convenient to characterize the depth of the correlation hole through the difference between inverse quantities  $|\frac{1}{S_{P\min}} - \text{PR}|$ . For GOE matrices, this difference is  $|\frac{1}{S_{P\min}} - \text{PR}| \approx \mathcal{D}/6 = \mathcal{D}_{\text{GOE}}/2$ . This alternative measure will prove useful as a dynamical witness to distinguish chaotic from integrable regimes.

As we will show, the survival probability — and particularly the depth of its correlation hole — is the clearest and most robust dynamical indicator of the transition between regularity and chaos. We compare the behavior of the correlation-hole depth with that of two local dynamical observables, the entanglement entropy and the imbalance, in order to obtain a reliable dynamical witness of the regular–chaos transition.

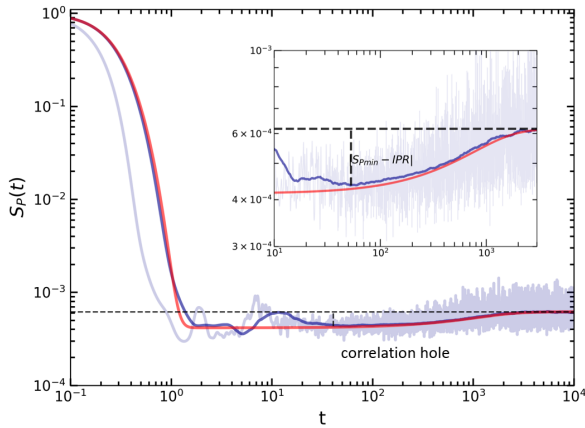


Figure 6. Averaged Survival Probability for an ensemble of 200 Fock states (light blue line) near the center of the spectrum. The inset shows the beginning and end of the correlation hole, for  $N = 8$ , the Hamiltonian parameters are in the most chaotic region  $U = D = 0.5J$ . The dark blue line is a moving average, the red line is the analytical curve averaged over those 200 Fock states, the horizontal dashed line is the relaxation value or IPR and the vertical dashed line in the inset is the depth of the correlation hole respect to the IPR

### B. Dynamics of the survival probability, entanglement entropy and imbalance

In this section, we analyze chaotic and regular dynamics by studying the evolution of the survival probability, entanglement entropy and imbalance as a functions of the interaction strength  $U$  or tilt  $D$ , for four different system sizes. Despite their distinct physical nature, all three observables display qualitatively similar behavior across the transitions between regular and chaotic regimes.

#### 1. Dynamics under tilt variation

The left panels of Fig. 7 present the dynamics of the three observables as the tilt is varied: the survival probability, the averaged one-site entanglement entropy and the half-chain imbalance. For each observable, the time intervals shown were chosen such that equilibration is reached.

Panel (a) displays the evolution of the survival probability  $S_P(t)$  in log-log scale and reveals two key features. First, for small  $D/J$  (the first two curves), a correlation hole develops at intermediate times  $t \in [20, 10^3]$ . This feature disappears as the tilt increases and becomes fully suppressed for  $D \geq 1.6J$ . Second, as the tilt grows, a pronounced revival emerges after the initial quadratic decay. We attribute these revivals to Bloch oscillations, which dominate the dynamics once the tilt becomes sufficiently strong [23].

The entanglement entropy, plotted in panel (b), also exhibits these oscillations following its initial rapid growth. Because the vertical axis uses a linear scale, the

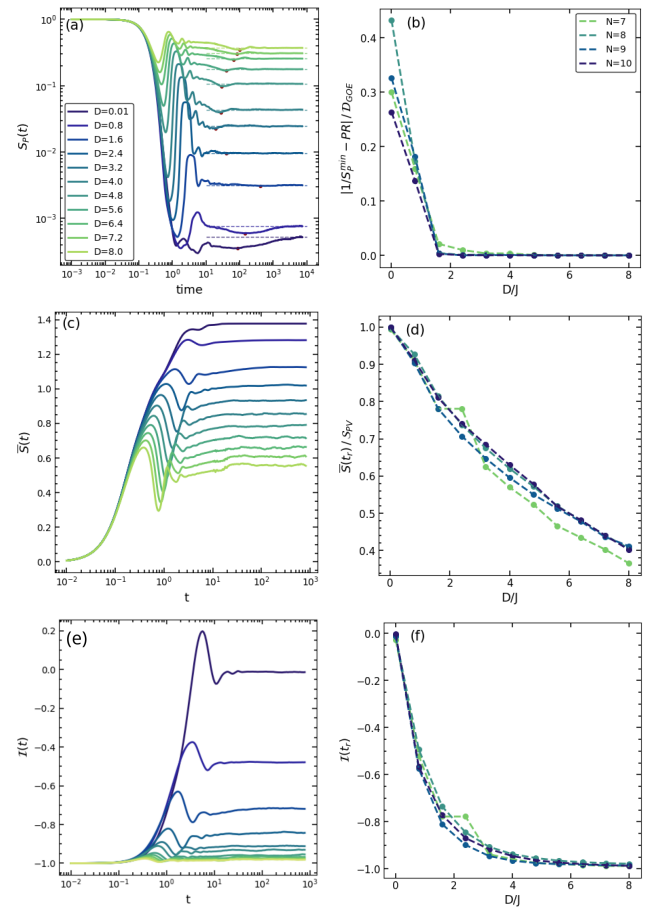


Figure 7. Averaged evolutions of (a) Survival probability  $S_P(t)$ , (c) entanglement entropy and (e) half chain imbalance for  $N = 8$  and fixed interaction  $U/J = 0.5$ . Each curve is the average over 50 Fock states (Survival Probability averaged over 200 states) at the center of the spectrum with states initially prepared with  $n_{max} = 3$  bosons per site for different values of the tilt  $D$ . In the case of imbalance, we chose states with the same initial imbalance  $I(t_0) = -1$ , which corresponds to 0 bosons to the left and  $M$  to the right part of the chain. All the curves were smoothed with a moving average. On the right panel: (b), (c), (d) we show the relaxation values (averaged over the last 10 values of the evolution) of the observables for different scales; in the case of the survival probability we show the depth of the correlation hole for different scales by scaling with the participation ratio.

strengthening of the oscillations with increasing tilt becomes even more evident, further supporting their interpretation as Bloch oscillations. Note that the two curves corresponding to the chaotic regime (small tilt) lie very close together and reach the highest equilibration values. As the tilt increases and the system exits the chaotic regime ( $D \geq 1.6J$ ), the equilibration value of the entanglement entropy decreases, making this observable a sensitive indicator of the transition from chaos to integrability. However, as we will discuss below, the depth of the correlation hole provides an even sharper probe of this transition, as seen by comparing panels (b) and (d)

of Figure 7.

Panel (b) shows, as a function of the tilt and for four different system sizes, the ratio between the correlation-hole depth,  $|\frac{1}{S_{P_{min}}} - PR|$ , and the dimension of the Hilbert space,  $\mathcal{D}_{GOE} = \mathcal{D}/3$ , while panel (d) presents the same but for the equilibration value of the entanglement entropy normalized by the respective Page value. A first key observation of both panels is that, after the appropriate rescaling —by the Hilbert-space dimension for the correlation-hole depth and by the Page value for the entanglement entropy—the curves collapse onto nearly identical shapes across system sizes. This collapse indicates universal behavior. Likewise, both panels highlight that the depth of the correlation hole is a significantly more sensitive indicator of the transition from chaotic to regular dynamics: it drops sharply from a finite value to nearly zero around  $D/J \approx 1.6$ , in agreement with the analysis based on the mean level-spacing ratio in Fig.1. In contrast, the equilibration value of the entanglement entropy also decreases with increasing tilt, but with a much smoother trend. It is also worth noting that in the most chaotic case ( $D = 0.01J$ ), which exhibits the deepest correlation hole in panel (b), the equilibration value of the entanglement entropy saturates at Page value, given analytically in Eq. (7).

Panels (e) and (f) of Fig. 7 show the corresponding results for the imbalance. Panel (e) displays its dynamics, averaged over Fock states with initial half-chain imbalance  $\mathcal{I}_0 = -1$ . Panel (f) displays the equilibrium values as a function of tilt for four different system sizes. The imbalance dynamics resembles that of the entanglement entropy: an initial rapid growth followed by oscillations, although in this case oscillations already appear at small tilt. For the smallest tilt values, the imbalance equilibrates close to zero,  $\mathcal{I}(t_{relax}) = 0$ . As the tilt increases, the equilibrium value decreases significantly, reaching  $\mathcal{I}(t_{relax}) \approx -0.5$  for  $D = 0.8$ . This value continues to decrease as the tilt grows and the system crosses into the regular regime. For large tilt, the equilibrium imbalance remains close to its initial value, approaching  $\mathcal{I}(t_{relax}) \approx -1$ , characteristic of Wannier-Stark localization. Thus, the decrease in the equilibrium imbalance reflects the transition from a chaotic regime at small tilt to the regular Wannier-Stark Localization regime at large tilt.

## 2. Dynamics under interaction variation

Figure 8 presents the results obtained when varying the interaction strength at fixed tilt  $D = 0.5J$ . In all cases, the survival probability in panel (a) displays an initial quadratic decay which —unlike the tilt-varying case —is not followed by strong oscillations. From weak to intermediate interactions ( $U \in [0.5, 2.4]$ ), a clear correlation hole is visible in the first three curves. As  $U/J$  increases, the correlation-hole gradually disappears, and the survival probability decays directly towards its relaxation

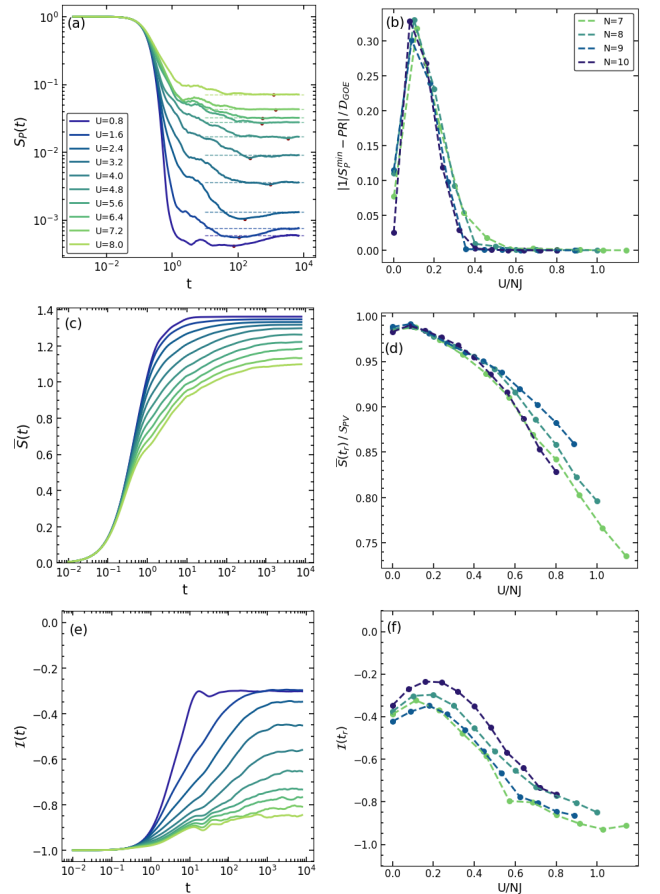


Figure 8. Same observables as Fig. 7 but changing the interaction  $U$ , with  $D/J = 0.5$

value, set by the IPR.

Panel (c) shows the dynamics of the averaged one-site entanglement entropy. For chaotic cases, the entropy grows rapidly and reaches a high equilibrium value. As  $U$  increases and the system crosses to the regular hardcore bosons regime, the equilibration value decreases and the equilibration time grows exponentially. The imbalance dynamics in panel (e) shows similar behavior: chaotic cases reach larger equilibration values at significantly shorter times, whereas stronger interactions lead to slower relaxation and lower stationary imbalance.

The right panels of Fig.8 show the depth of the correlation hole and the equilibrium values of the entanglement entropy and imbalance as functions of the interaction strength for different system sizes. As before, once observables are properly rescaled, the curves for all four system sizes collapse onto very similar trends. The interaction strength on the horizontal axes is scaled by the number of particles, consistent with the two-body character of the interaction term.

Note that in the right panels, unlike the left ones, we also include results for a very small interaction ( $U/J = 0.01$ ), corresponding to the regular Wannier-Stark localization regime. This is reflected in the fact that

the curves for the three observables exhibit a maximum at  $U/(NJ) \sim 0.15$ . Once again, the depth of the correlation-hole provides the sharpest and more reliable indicator of the chaotic regime. Although the equilibrium entanglement entropy and imbalance also capture the transition, their variations are noticeably smoother. For all system sizes, the entanglement entropy reaches its maximum—the Page value—at the same interaction strength where the correlation hole is deepest. However, its decrease is much more gradual than the sharp drop observed in the correlation-hole depth. In contrast, the equilibrium imbalance exhibits a steeper decline than the entanglement entropy, but its maximum occurs at slightly larger interaction strength than the one at which the correlation-hole depth is maximal.

## V. CONCLUSIONS

In this work we investigated the one-dimensional tilted Bose–Hubbard model with open boundary conditions and showed that the competition between the interaction term and the linear tilt generates a rich dynamical landscape spanning ergodic quantum chaos and integrable, non-ergodic behavior. Two prominent limits structure this landscape: the Wannier–Stark localization (WSL) regime and the hard-core bosons (HCB) regime. On the static side, spectral diagnostics based on the mean ratio of consecutive level-spacings delineate the crossover between chaotic and regular regions across parameter space. This spectral picture is corroborated by eigenstate-based indicators, including the participation ratio in the Fock basis and the one-site-averaged entanglement entropy, which display clear qualitative changes when moving between chaotic domains (characterized by relatively uniform eigenstate properties) and regular domains (where eigenstate indicators become strongly dispersed and structured).

On the dynamical side, we found that the survival probability  $S_P(t)$ —and, in particular, the depth of its correlation hole—provides the sharpest and most direct dynamical witness of chaos throughout both crossovers, i.e., from chaos towards WSL and from chaos towards HCB. In the chaotic regime,  $S_P(t)$  exhibits the characteristic dip–ramp–plateau behavior associated with long-range spectral correlation, and the correlation-hole depth follows the expected scaling with Hilbert-space size, consistent with GOE expectations. As the system becomes regular, the correlation hole disappears, yielding a clean dynamical signature of the loss of spectral rigidity.

These conclusions are broadly consistent with the behavior of two experimentally accessible observables: the on-site entanglement entropy and the half-chain imbalance. In the tilt-dominated (WSL) regime ( $D/J \gg U/J$ ), the dynamics is marked by pronounced oscillations consistent with Bloch oscillations, the absence of a correlation hole in  $S_P(t)$ , reduced long-time entanglement, and an effective freezing of the imbal-

ance near its initial value. In the interaction-dominated (HCB) limit ( $U/J \gg D/J$ ), Bloch oscillations are absent, but the remaining signatures of regular dynamics persist: relaxation slows down, entanglement equilibrates to lower values, and the imbalance retains strong memory of the initial condition. By contrast, when tilt and interactions are comparable, the system enters an extended chaotic regime in which the correlation hole becomes visible, the entanglement entropy rapidly approaches the analytically available Page value, and the imbalance relaxes toward values close to zero, consistent with efficient redistribution of particles across the chain.

Importantly, the equilibrium (long-time) values of all three dynamical probes track the regular-to-chaotic crossover and—once appropriately rescaled—exhibit universal trends that are largely independent of system size. The entanglement entropy, in particular, becomes naturally comparable across sizes when normalized by the corresponding Page value, revealing a robust scaling collapse. Among all observables considered, the survival probability remains the most reliable and sensitive indicator of chaos, because it directly encodes long-range spectral correlations through the correlation hole. Interestingly, we also find that the imbalance provide a sharper contrast than entanglement entropy across parts of the crossover, despite entanglement being the more standard diagnostic of thermalization.

Overall, our results establish the correlation hole in the survival probability as a stringent dynamical marker of chaos in the tilted Bose–Hubbard model, while entanglement and imbalance provide complementary, experimentally accessible signatures. The observed scaling collapses suggest a universal description of the chaos–regular crossover that persists across system sizes and particle numbers.

## ACKNOWLEDGMENTS

We acknowledge the support of the Computation Center - ICN, in particular to Enrique Palacios, Luciano Díaz, and Eduardo Murrieta. C.D-M. and J.G.H acknowledge partial financial support from the DGAPA-UNAM projects IN109523 and IN101526.

## Appendix A: Set of initial Fock states and scaling of the chaos transition

In this appendix, we provide additional details on the set of initial Fock states used to study the dynamics of entanglement entropy and imbalance, illustrated for the case  $N = M = 8$ .

Figures 9 and 10 show, for varying tilt and interaction strength, the mean energy and participation ratio in the Hamiltonian eigenbasis of the selected initial Fock states. The states used to study entanglement entropy are marked with blue dots across all panels, while those

used for imbalance are indicated with red dots. For reference, the participation ratio of the respective Hamiltonian eigenstates in the Fock basis is plotted against their rescaled energies using gray dots.

The initial Fock states for entanglement entropy were chosen as 50 random states located near the center of the spectrum for  $U = 0.5J$  and  $D = 0.8J$ . This explains why the blue dots in the top-right panel of Fig. 9 cluster around the middle-energy region. In the other panels, the blue dots spread across the energy range, though they remain close to the region where Hamiltonian eigenstates exhibit larger participation ratios.

By contrast, states with a fixed initial imbalance of  $\mathcal{I}(0) = -1$  tend to shift towards the high-energy edge of the spectrum. As a result, these states undergo localization in the Hamiltonian eigenbasis more rapidly than those selected from the spectral center. This spectral migration accounts for the faster decay of imbalance relaxation values compared to those of the entanglement entropy as tilt or interaction strength increases.

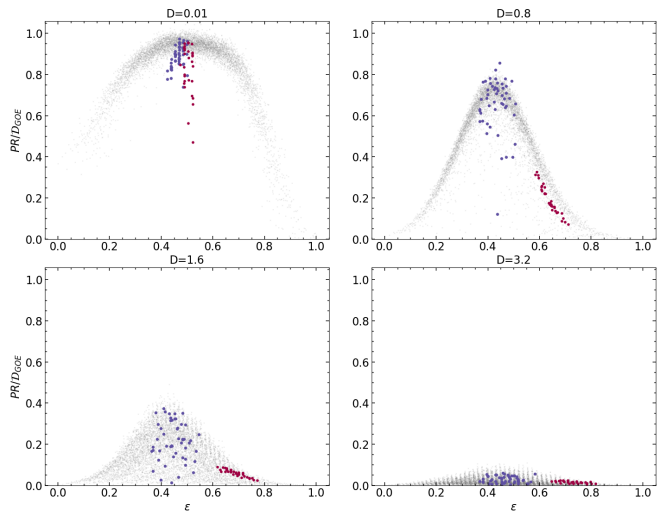


Figure 9. Distribution of the Participation ratio (PR) of eigenstates in the Fock basis (light gray background) for different tilt values at fixed interaction  $U/J = 0.5$ , with  $N = M = 8$ , as a function of their normalized eigenenergies  $\epsilon$ . Blue dots indicate the mean energy and participation ratio in the energy eigenbasis of the 50 random initial Fock states used to study the dynamics of entanglement entropy. Red dots represent correspond to the set of 31 initial states with fixed initial imbalance  $\mathcal{I}(0) = -1$ . All states are restricted to a maximum site occupation of  $n_i \leq 3$  bosons.

Finally, in Fig. 11, we present a finite-size scaling analysis of the mean level spacing ratio to test the robustness

of the transition between regular and chaotic regimes against changes in system size. This analysis supports the static phase diagram shown in Fig. 1, revealing no significant dependence on system size within the studied range  $N \in [8, 9, 10]$ . It is worth noting that, consistent with other similar scaling analyses in the main text, the dependence of  $\langle r \rangle$  on the interaction strength (right

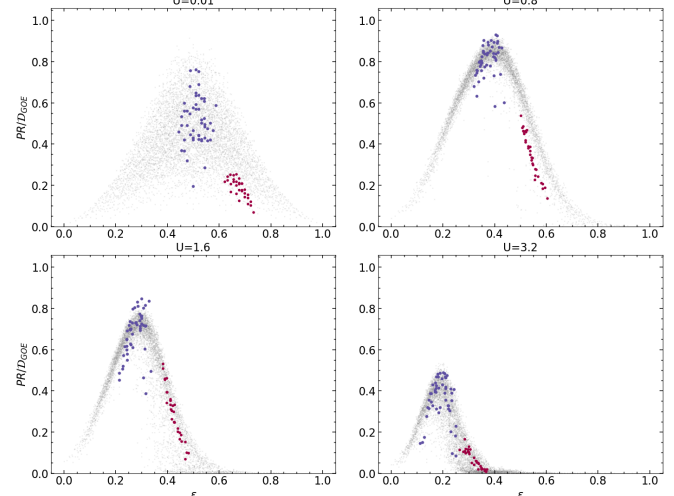


Figure 10. Same analysis as in Fig. 9, but varying the interaction strength at a fixed tilt  $D/J = 0.5$ .

panel) was normalized by the number of particles  $N$ , in agreement with the two-body nature of this interaction term.

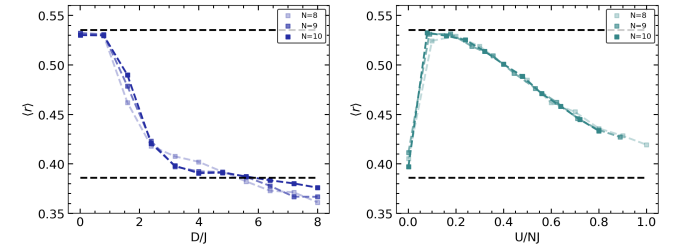


Figure 11. Mean level spacing ratio  $\langle r \rangle$  for different system sizes  $N \in [8, 9, 10]$ . The green curves (right panel) represent the change in interaction  $U$  (at fixed tilt), while the blue curves (left panel) represent the change in tilt  $D$  (at fixed interaction). The upper and lower black dashed lines indicate the theoretical values for the GOE ( $\langle r \rangle_{\text{GOE}} \approx 0.536$ ) and Poisson ( $\langle r \rangle_{\text{P}} \approx 0.386$ ) limits, respectively.

---

[1] Mark Srednicki. Chaos and thermalization in quantum many-body systems. *Phys. Rev. E*, 50:888–901, Aug 1994.

[2] Marcos Rigol, Vanja Dunjko, and Maxim Olshanii. Thermalization in a strongly interacting one-dimensional bose gas. *Nature*, 452(7189):854–858, 2008.

[3] F. Borgonovi, F. M. Izrailev, L. F. Santos, and V. G. Zelevinsky. Quantum chaos and thermalization in isolated systems of interacting particles. *Phys. Rep.*, 626:1–58, 2016.

[4] Luca D’Alessio, Yevgeny Kafri, Anatoli Polkovnikov, and Marcos Rigol. From quantum chaos and eigenstate thermalization to statistical mechanics and thermodynamics. *Adv. Phys.*, 65(3):239–362, 2016.

[5] Pilar Martín Clavero and Alberto Rodríguez. Characterization of the chaotic phase in the tilted bose-hubbard model. *Phys. Rev. E*, 111:064214, Jun 2025.

[6] Andreas Buchleitner and Andrey R. Kolovsky. Interaction-induced decoherence of atomic bloch oscillations. *Phys. Rev. Lett.*, 91:253002, Dec 2003.

[7] Marianne Theresia Viktoria Schneider, A Rodríguez, and A Buchleitner. *Fock Space Localization of Many-Body States in the Tilted Bose-Hubbard Model*. PhD thesis, Universität, 2019.

[8] Lukas Beringer, Mathias Steinhuber, Juan Diego Urbina, Klaus Richter, and Steven Tomsovic. Controlling many-body quantum chaos: Bose–hubbard systems. *New Journal of Physics*, 26(7):073002, 2024.

[9] Qiujiang Guo, Chen Cheng, Hekang Li, Shibo Xu, Pengfei Zhang, Zhen Wang, Chao Song, Wuxin Liu, Wen-hui Ren, Hang Dong, et al. Stark many-body localization on a superconducting quantum processor. *Physical review letters*, 127(24):240502, 2021.

[10] Yong-Yi Wang, Zheng-Hang Sun, and Heng Fan. Stark many-body localization transitions in superconducting circuits. *Physical Review B*, 104(20):205122, 2021.

[11] S. R. Taylor, M. Schulz, F. Pollmann, and R. Moessner. Experimental probes of stark many-body localization. *Phys. Rev. B*, 102:054206, Aug 2020.

[12] M. Greiner, O. Mandel, T. Esslinger, T. W. Hänsch, and I. Bloch. Quantum phase transition from a superfluid to a mott insulator in a gas of ultracold atoms. *Nature*, 415(6867):39–44, 2002.

[13] Alexander Lukin, Matthew Rispoli, Robert Schittko, M. Eric Tai, Adam M. Kaufman, Soonwon Choi, Vedika Khemani, Julian Léonard, and Markus Greiner. Probing entanglement in a many-body-localized system. *Science*, 364(6437):256–260, 2019.

[14] Fritz Haake. *Quantum Signatures of Chaos*. Springer, Berlin, 3 edition, 2010.

[15] E. J. Torres-Herrera and Lea F. Santos. Dynamical manifestations of quantum chaos: correlation hole and bulge. *Philosophical Transactions of the Royal Society A: Mathematical, Physical and Engineering Sciences*, 375(2108):20160434, 2017.

[16] Eduardo Jonathan Torres-Herrera and Lea F. Santos. Signatures of chaos and thermalization in the dynamics of many-body quantum systems. *The European Physical Journal Special Topics*, 227(15):1897–1910, Mar 2019.

[17] Javier de la Cruz, Sergio Lerma-Hernández, and Jorge G. Hirsch. Quantum chaos in a system with high degree of symmetries. *Phys. Rev. E*, 102:032208, Sep 2020.

[18] M. Schulz, C. A. Hooley, R. Moessner, and F. Pollmann. Stark many-body localization. *Phys. Rev. Lett.*, 122:040606, Jan 2019.

[19] William Morong, Fangli Liu, Patrick Becker, KS Collins, Lei Feng, Antonis Kyprianidis, Guido Pagano, Tianyu You, AV Gorshkov, and Christopher Monroe. Observation of stark many-body localization without disorder. *Nature*, 599(7885):393–398, 2021.

[20] Pedro Ribeiro, Achilleas Lazarides, and Masudul Haque. Many-body quantum dynamics of initially trapped systems due to a stark potential: Thermalization versus bloch oscillations. *Phys. Rev. Lett.*, 124:110603, Mar 2020.

[21] D. Jaksch, C. Bruder, J. I. Cirac, C. W. Gardiner, and P. Zoller. Cold bosonic atoms in optical lattices. *Phys. Rev. Lett.*, 81:3108–3111, Oct 1998.

[22] Andrey R Kolovsky. New bloch period for interacting cold atoms in 1d optical lattices. *Physical review letters*, 90(21):213002, 2003.

[23] Florian Meinert, Manfred J Mark, Emil Kirilov, Katharina Lauber, Philipp Weinmann, Michael Gröbner, and H-C Nägerl. Interaction-induced quantum phase revivals and evidence for the transition to the quantum chaotic regime in 1d atomic bloch oscillations. *Physical Review Letters*, 112(19):193003, 2014.

[24] Timo Hartmann, F Keck, HJ Korsch, and S Mossmann. Dynamics of bloch oscillations. *New Journal of Physics*, 6(1):2, 2004.

[25] Lukas Pausch, Andreas Buchleitner, Edoardo G Carnio, and Alberto Rodríguez. Optimal route to quantum chaos in the bose–hubbard model. *Journal of Physics A: Mathematical and Theoretical*, 55(32):324002, 2022.

[26] Vadim Oganesyan and David A. Huse. Localization of interacting fermions at high temperature. *Phys. Rev. B*, 75:155111, Apr 2007.

[27] Rahul Nandkishore and David A. Huse. Many-body localization and thermalization in quantum statistical mechanics. *Annual Review of Condensed Matter Physics*, 6(1):15–38, 2015.

[28] Carlos Diaz-Mejia, Javier de la Cruz, Sergio Lerma-Hernández, and Jorge G Hirsch. Persistent revivals in a system of trapped bosonic atoms. *Physics Letters A*, 493:129262, 2024.

[29] L Kaplan, F Leyvraz, C Pineda, and T H Seligman. A trivial observation on time reversal in random matrix theory. *Journal of Physics A: Mathematical and Theoretical*, 40(49):F1063, nov 2007.

[30] Angelo Piga, Maciej Lewenstein, and James Q Quach. Quantum chaos and entanglement in ergodic and nonergodic systems. *Physical Review E*, 99(3):032213, 2019.

[31] Guo-Xian Su, Hui Sun, Ana Hudomal, Jean-Yves Desaules, Zhao-Yu Zhou, Bing Yang, Jad C Halimeh, Zhen-Sheng Yuan, Zlatko Papić, and Jian-Wei Pan. Observation of many-body scarring in a bose-hubbard quantum simulator. *Physical Review Research*, 5(2):023010, 2023.

[32] Yale Yauk, Rohit Patil, Yicheng Zhang, Marcos Rigol, and Lucas Hackl. Typical entanglement entropy in systems with particle-number conservation. *Physical Review B*, 110(23):235154, 2024.

[33] Ruixiao Yao and Jakub Zakrzewski. Many-body localization of bosons in an optical lattice: Dynamics in disorder-free potentials. *Phys. Rev. B*, 102:104203, Sep 2020.

[34] Evert van Nieuwenburg, Yuval Baum, and Gil Refael. From bloch oscillations to many-body localization in clean interacting systems. *Proceedings of the National Academy of Sciences*, 116(19):9269–9274, 2019.

[35] Sebastian Scherg, Thomas Kohlert, Pablo Sala, Frank Pollmann, Bharath Hebbe Madhusudhana, Immanuel Bloch, and Monika Aidelsburger. Observing non-ergodicity due to kinetic constraints in tilted fermi-hubbard chains. *Nature Communications*, 12(1):4490, 2021.

- [36] Ling-Na Wu and André Eckardt. Bath-induced decay of stark many-body localization. *Physical Review Letters*, 123(3):030602, 2019.
- [37] Hyungwon Kim and David A Huse. Ballistic spreading of entanglement in a diffusive nonintegrable system. *Physical review letters*, 111(12):127205, 2013.
- [38] Maksym Serbyn, Zlatko Papić, and Dmitry A Abanin. Universal slow growth of entanglement in interacting strongly disordered systems. *Physical review letters*, 110(26):260601, 2013.
- [39] E. Brézin and S. Hikami. Spectral form factor in a random matrix theory. *Phys. Rev. E*, 55:4067–4083, Apr 1997.
- [40] Y. Alhassid and R. D. Levine. Spectral autocorrelation function in the statistical theory of energy levels. *Phys. Rev. A*, 46:4650–4653, Oct 1992.
- [41] E. J. Torres-Herrera and L. F. Santos. Dynamics of a many-body localized system and the transition to a thermal phase. *Phys. Rev. E*, 92:032912, Sep 2015.
- [42] Mauro Schiulaz, E Jonathan Torres-Herrera, and Lea F Santos. Thouless and relaxation time scales in many-body quantum systems. *Physical Review B*, 99(17):174313, 2019.